High-definition imaging of carotid artery wall dynamics

Kruizinga, Pieter; Mastik, Frits; van den Oord, Stijn C.H.; Schinkel, Arend F.L.; Bosch, Johannes G.; de Jong, Nico; van Soest, Gijs; van der Steen, Anton F.W.

DOI
10.1016/j.ultrasmedbio.2014.03.009

Publication date
2014

Document Version
Final published version

Published in
Ultrasound in Medicine and Biology

Ultrasound in Med. & Biol., Vol. 40, No. 10, pp. 2392–2403, 2014

0301-5629/$ - see front matter

http://dx.doi.org/10.1016/j.ultrasmedbio.2014.03.009

● *Original Contribution*

HIGH-DEFINITION IMAGING OF CAROTID ARTERY WALL DYNAMICS

Pieter Kruizinga,* Frits Mastik,* Stijn C. H. van den Oord,*† Arend F. L. Schinkel,† Johannes G. Bosch,* Nico de Jong,*‡§ Gijs van Soest,* and Anton F. W. van der Steen*‡§||

*Department of Biomedical Engineering, Thoraxcenter, Erasmus MC, Rotterdam, The Netherlands; †Department of Cardiology, Thoraxcenter, Erasmus MC, Rotterdam, The Netherlands; ‡Interuniversity Cardiology Institute, Utrecht, The Netherlands; §Delft University of Technology, Delft, The Netherlands; and ||Shenzhen Institutes of Advanced Technology, Chinese Academy of Sciences, Shenzhen, China

(*Received* 11 *December* 2013; *revised* 12 *February* 2014; *in final form* 10 *March* 2014)

Abstract—The carotid artery (CA) is central to cardiovascular research, because of the clinical relevance of CA plaques as culprits of stroke and the accessibility of the CA for cardiovascular screening. The viscoelastic state of this artery, essential for clinical evaluation, can be assessed by observing arterial deformation in response to the pressure changes throughout the cardiac cycle. Ultrasound imaging has proven to be an excellent tool to monitor these dynamic deformation processes. We describe how a new technique called high-frame-rate ultrasound imaging captures the tissue deformation dynamics throughout the cardiac cycle in unprecedented detail. Local tissue motion exhibits distinct features of sub-micrometer displacements on a sub-millisecond time scale. We present a high-definition motion analysis technique based on plane wave ultrasound imaging able to capture these features. We validated this method by screening a group of healthy volunteers and compared the results with those for two patients known to have atherosclerosis to illustrate the potential utility of this technique. (E-mail: p.kruizinga@erasmusmc.nl) **© 2014 World Federation for Ultrasound in Medicine & Biology.**

Key Words: **Plane wave imaging, High-frame-rate ultrasound, Carotid artery, Tissue Doppler, Pulse wave velocity.**

INTRODUCTION

The healthy artery wall is a layered structure with nonlinear elastic properties that enable it to sustain rapid and large variations in blood pressure (Shadwick 1999). Muscular arteries, such as the carotid and coronary arteries, respond actively and passively to the systemic pressure cycle, adapting their diameter or tone to physiologic circumstances. Under the influence of age and chemical and mechanical stresses, the artery wall may be affected by atherosclerosis, a systemic inflammatory disease that leads to the formation of plaques consisting of calcifications and lipid-rich necrotic material. Lipid-rich plaques may become unstable and rupture, in which case an atherothrombotic reaction can lead to cerebral or cardiac ischemic events (Carr et al. 1996; Schaar et al. 2003; Shoji et al. 2010; van Popele et al. 2001). Advanced atherosclerosis also compromises vascular function and the elastic response of the arteries in a phenomenon known as arterial stiffening. Loss of elasticity of the arterial wall may result in systemic arterial hypertension (O'Rourke et al. 2002). A full assessment of vascular elasticity, as well as plaque stability, requires mapping of the local biomechanical properties of the artery wall: Atherosclerosis is heterogeneous in its prevalence and severity. Soft plaques are more liable to rupture than stiff ones (de Korte et al. 2002; Grønholdt 1999; Shah 2003), and arterial stiffness varies throughout the body. Local biomechanics can be probed by imaging the tissue velocity in response to the systemic pressure variations.

Those local variations are critical to plaque stability: A rupture will occur if the weakest point lacks sufficient strength to withstand the applied stress, a condition that cannot be gauged by average measurements (Cheng et al. 1993; de Korte et al. 2002; Schaar et al. 2003). Locations with large tissue strain are particularly liable to rupture. The amount of tissue deformation can be obtained by measuring the tissue velocity under varying load (D'Hooge et al. 2000; Heimdal et al. 1998; Schmidt-Trucksäss et al. 1998). In this paper we aim to measure the tissue velocity of the carotid artery (CA) wall. The CA is important because of its high incidence of atherosclerosis, its strong association with cerebrovascular

Address correspondence to: Pieter Kruizinga, PO Box 2040, 3000 CA Rotterdam, The Netherlands. E-mail: p.kruizinga@erasmusmc.nl

events (Grønholdt et al. 2001; Laurent et al. 2006) and the relation between atherosclerosis in the CA and atherosclerosis in other vascular beds, such as the coronary arteries (Hellings et al. 2010; Inaba et al. 2012; Lorenz et al. 2007; Triposkiadis et al. 2005). The CA is also superficially located, making it an ideal imaging target for screening applications.

Arteries can become stiff, losing the ability to support large and rapid pressure variations. The most reliable indicator of arterial stiffness is thought to be arterial pulse wave velocity (PWV) obtained with ultrasound (US) echo tracking (Asmar et al. 1995; Benthin et al. 1991; Hoeks et al. 1990; Laurent et al. 2006; O'Rourke et al. 2002). The propagation speed of the pulse wave (PW), a pressure wave generated by the heart in systole, can be related to arterial elasticity using the Moens–Korteweg equation (Korteweg 1878), whereby stiffening of the arterial wall causes the PW to propagate faster (Hermeling et al. 2007). In recent years, several research groups have refined the quantification of the PWV in the CA using high-frame-rate (HFR) ultrasound (Couade et al. 2011; Eriksson et al. 2002; Hasegawa et al. 2013; Hermeling et al. 2009; Kanai et al. 2000; Luo et al. 2012; Sorensen et al. 2008). Although the techniques developed in these studies adequately measure PWV, they do not transcend the limitation of using a single parameter to describe the overall elastic state of a complete arterial segment, in this case the CA. Such a single parameter assumes a constant elastic state throughout the cardiac cycle and a constant elastic state across the whole region. These two assumptions ignore two important observations. First, because the elastic state of the artery wall varies with blood pressure (Shadwick 1999) and heart rate (Lantelme et al. 2002), the propagation of the arterial pulse wave is non-linear (Couade et al. 2010; Fung 1993). Second, applying an average PWV to an entire arterial segment does not allow for the assessment of local variations in the elastic properties within the wall (Shahmirzadi and Konofagou 2012).

Accurate assessment of arterial disease thus necessitates local evaluation of the tissue dynamics. The typical length scales and tissue velocities involved lead to requirements of high temporal and spatial resolution. In the case of the CA, we want to image the interaction of the incoming phase of any arterial PW with the CA wall over some distance. Considering a PWV of several meters per second (Koivistoinen et al. 2007) and an interaction length on the order of millimeters, we require a modality that can provide frame rates on the order of kilohertz. Given that the tissue velocity during PW interactions is only a few millimeters per second (Eriksson et al. 2002; Luo et al. 2012), we require that the modality is capable of measuring sub-micron displacement. The only imaging tool available today that can fulfill both requirements is HFR ultrasound imaging (Ekroll et al. 2013; Hasegawa and Kanai 2008; Lu 1997; Tanter et al. 2002; Udesen et al. 2008).

Here we present a high-definition motion-analysis technique based on plane-wave US imaging, which allows us to visualize arterial wall dynamics at short time and small spatial scales. We measure arterial wall motion on the basis of instantaneous phase echo differences between successive frames obtained with plane wave US imaging. We illustrate that the first-order difference of the instantaneous phase of the beamformed signals provides an efficient way to measure tissue motion locally. With this method, we can now capture the full dynamics of pressure waves interacting with the CA wall. To test our method, we scanned a group of healthy volunteers ($n = 23$) and patients with CA arteriosclerosis ($n = 2$) using HFR US imaging at an average frame rate of 4.6 kHz. We illustrate that motion in a diseased artery wall with plaque is different from the motion observed in a healthy artery. We also provide proof that this technique can be used to obtain the PWV. The validity of the proposed motion derivation is indicated by the reproducibility and consistency over the volunteers, over several cardiac cycles per volunteer and frame-to-frame motion.

METHODS

With the US technique, the resolution of delay estimation is very good in the direction of the transmit beam (axial motion) and is poor in the direction perpendicular to the beam (lateral motion). We therefore decided to restrict ourselves to axial motion, although it should be noted that there are techniques that can measure the complete tissue displacement vector with US imaging (Ekroll et al. 2013; Jensen and Munk 1998; Tanter et al. 2002). Fortunately, the lateral motion of the CA wall in the longitudinal view is predominantly slow (induced by, *e.g.*, breathing) and easily separated from the rapidly changing axial motion, with the latter intrinsically related to arterial distension (Golemati et al. 2003; Zahnd et al. 2013).

Ultrasound imaging relies on the detection of ultrasonic pulses reflected (and backscattered) by tissue. When tissue moves, the next resulting reflection exhibits a delay with respect to the earlier echoes. Measuring this delay provides a direct tool for assessing tissue motion. Delay estimation in US is often done by cross-correlating the received echoes (Lubinski et al. 1999). Instead of cross-correlating the echoes, we can also use the phase of the signals to determine the delays. The phase can be unwrapped to obtain a measure of the exact location of the echoes along each image line, as proposed by Wilson and Robinson (1982). However, unwrapping may introduce errors as a result of noise when the phase

is close to $\pm\pi$. Instead of unwrapping the phase, we can also apply a first-order time difference along the frame dimension. When the phase change between two successive frames is $\leq\pm\pi$, we obtain a direct measure of tissue motion that is directly related to the Doppler shift, as was reported by Hartley et al. (1991). The $\leq\pm\pi$ coherency condition translates into a HFR requirement. In the case of HFR US imaging of the carotid artery, we not only easily satisfy the frame rate condition, but also have a large number of phase samples available (in both space and time), which makes the phase-difference method once more worthy of consideration.

Phase-difference method

The phase-difference method comprises five different steps.

1. We apply beamforming to the received radiofrequency (RF) signals after transmitting plane waves in the tissue. The beamforming is done in the Fourier domain, which can be very computationally effective (Cheng and Lu 2006; Kruizinga et al. 2012a). It requires a forward 2-D fast Fourier transform (FFT), an interpolation of the Fourier coefficients and an inverse Fourier transform. By zeroing the conjugate or negative part of the spectrum before back-transformation (equal to the Hilbert transform), one obtains the analytical beamformed signal, $R(t)$, which can be separated into magnitude and phase image by means of the equations

$$E(t) = \sqrt{\left(R_r^2(t)+R_i^2(t)\right)}, \quad (1)$$

$$\phi(t) = \arctan\left(\frac{R_i(t)}{R_r(t)}\right), \quad (2)$$

where $E(t)$ denotes the magnitude or envelope image, and $\phi(t)$ denotes the phase image. The signals $R_r(t)$ and $R_i(t)$ denote the real and imaginary parts of the analytical signal, respectively. Every image $E(t)$ and $\phi(t)$ is stored in a separate 3-D matrix. The envelope matrix is used to display conventional B-mode images and to mask the velocity images. The phase matrix is used for our motion analysis; see Figure 1 for a schematic representation of the 3-D phase matrix.

2. We obtain the first-order difference of the phase matrix along the frame dimension. This phase-time difference directly yields the velocity of every pixel at each time point.
3. The $\pm2\pi$ wrapping that remains after the first-order difference is corrected by subtracting 2π from all values $>\pi$ and adding 2π to all values $<-\pi$.
4. For further regularization, all random-phase values resulting from echoes below a certain envelope threshold are masked out. Non-physiologic velocity values resulting from noise are set to zero.
5. Because we assume a certain continuity between neighboring samples, we apply a smoothing filter to reduce high-frequency velocity noise, using a separable 3-D Gaussian convolution with a small kernel.

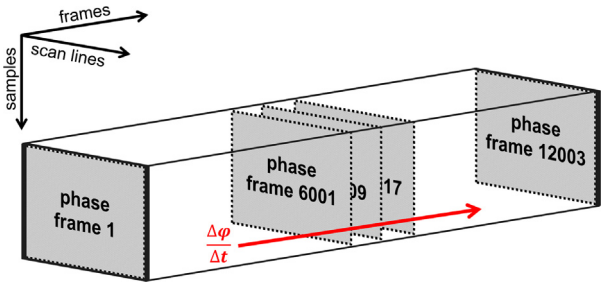

Fig. 1. Schematic impression of the 3-D phase-difference matrix.

Temporal integration along the frames yields local tissue displacement, whereas local acceleration may be obtained by a second differentiation.

The code described above was implemented in MATLAB 2012a (The MathWorks, Natick, MA, USA) with Jacket Version 2.0 (AccelerEyes, Atlanta, GA, USA) running on a 8-Core Intel Xeon 3.07-GHz workstation (Dell) with 48 Gb of memory and a GTX 680 4-Gb graphics card (NVIDIA, Santa Clara, CA, USA). This allowed for a throughput of about 2 min starting from 16 Gb raw RF data to the complete set of B-mode and tissue motion images. This period may be further shortened by choosing a different computing platform such as C/C++ or CUDA.

Carotid artery wall motion analysis

By measuring the distension of the CA in terms of displacement, velocity and acceleration, we gain insight into the elastic state of the artery as a whole and obtain values that can be used to calculate PWV locally, at every instant of the cardiac cycle. To this end, we defined separate regions of interest (ROIs) for the anterior and posterior wall. The first frame of the scan was used to define the positions of the ROIs. In MATLAB, two lines were manually aligned with the walls (using the routine *imdistline*). A fixed number of samples above and below these lines were then selected to provide the complete ROI. It was assumed the ROI included the wall during the complete scan. The advantage of using these ROIs was that 3-D phase processing could be further accelerated because only the samples within each ROI required processing. Based on the ROI selection, we derived a centerline for the lumen, whereby the pressure wave was assumed to propagate from right to left and along the direction of the centerline. Figure 2 provides a schematic overview of the ROI and centerline selection.

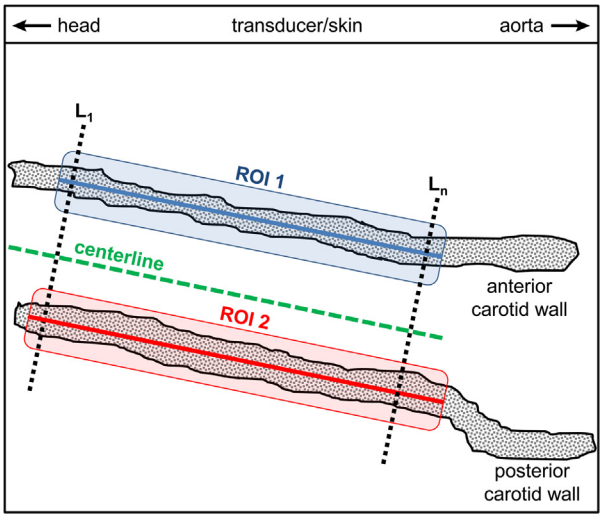

Fig. 2. Delineation of regions of interest for distension analysis. ROI = region of interest.

All samples along each image line ($L_1 \ldots L_n$ in Fig. 2) belonging to the ROI and the –30-dB fidelity mask were adjusted for the centerline angle and averaged. For every image line ($L_1 \ldots L_n$), a distension profile was obtained by subtracting the averaged samples of ROI 1 from ROI 2. This resulted in a total of N distensibility curves (represented in terms of velocity), where N is the number of scan lines present in both the anterior and posterior ROIs.

Pulse wave detection

Features within the arterial distension waveform, such as the systolic foot (SF) at the start of the distension waveform and the dicrotic notch (DN), which signals closure of the aortic valve, display transient behavior along the arterial wall and can therefore be used to obtain the PWV (Hermeling et al. 2009, 2011). PWV can be best estimated by comparing acceleration waveforms derived for every line perpendicular to the blood flow direction (Hermeling et al. 2011). In this study, we derived the PWV at the SF and DN. The acceleration waveforms were obtained by first-order difference of the computed distensibility curves and a 60-Hz low-pass fourth-order Butterworth filter to suppress the high-frequency noise (Hermeling et al. 2008). For every scan line, two peaks, corresponding to the SF and DN, in the acceleration profiles were identified (using the routine *findpeaks*). The slope of a least-squares regression line through the peak locations provided the PWV (see Fig. 6 for an example). For every scan, we averaged all SF PWV and DN PWV observations that gave a value within physiologic bounds 1 to 20 m/s.

In vivo *study*

In vivo validation of the proposed method was performed on a group of 23 healthy volunteers and on 2 patients known to have atherosclerosis. For each healthy volunteer, we scanned both CAs while the person was in supine position. We recorded blood pressure, height, weight and age. The two patients were scanned 1 d before undergoing endarterectomy surgery. All volunteers and patients gave written informed consent before HFR US scanning. The study was approved by the medical ethics committee of Erasmus Medical Centre, Rotterdam, The Netherlands.

Ultrasound equipment and software settings

The ultrasonic plane waves were transmitted using a broadband (4–9 MHz, –6-dB bandwidth) linear array consisting of 128 elements (Vermon, Tours, France). All elements were excited simultaneously with a two-cycle, 8-MHz Gaussian modulated sine pulse, with pressures well below the U.S. Food and Drug Administration limit. No surface heating of the array was observed. The array was interfaced with a 128-channel programmable ultrasound system using 12-bit, 80-MHz sampling (Lecoeur Electronique, Chuelles, France). Acquisition depth for each of the various volunteers and patients was varied between 20 and 32 mm. The scanning period was adjusted to the heart rate and set to obtain at least two complete heart cycles. Imaging frame rates from 4 to 7 kHz were realized through a trade-off between imaging depth, number of imaging frames and acquisition time. This system achieved a maximum frame rate of 35 kHz (Kruizinga et al. 2012b).

The plane wave preview mode provided a refresh rate of one frame per second, limited by the data transfer rate of the Lecoeur ultrasound system. As soon as a full longitudinal view of the CA was obtained, the HFR mode was activated and several thousand frames were acquired over a period of 2 to 3 s. After acquisition, the data were transferred from the ultrasound system to a powerful processing computer. The RF was bandpass filtered using a fourth-order Butterworth digital filter. Beamforming was done in the Fourier domain using complex linear interpolation and resampling to a 40-MHz grid (Kruizinga et al. 2012a). The envelope fidelity mask

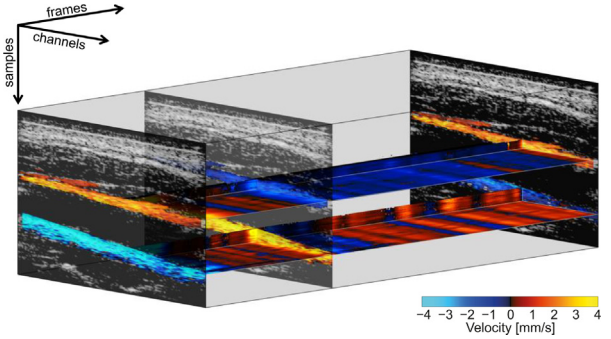

Fig. 3. Three-dimensional representation of carotid artery wall velocity for the period of half a heart cycle.

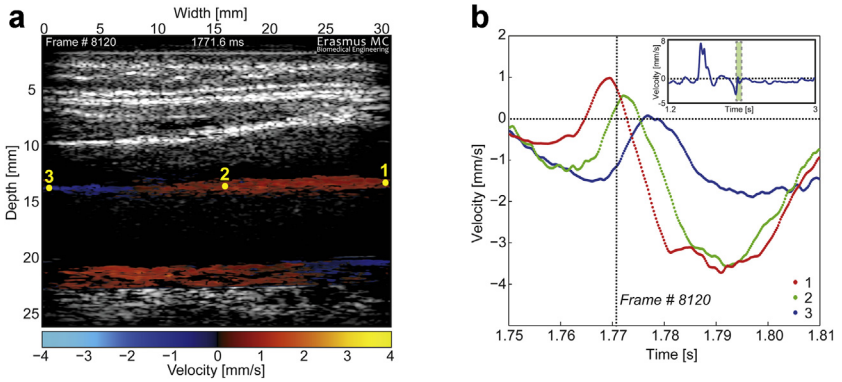

Fig. 4. Pixel unique tissue velocity profiles in a healthy artery wall. The three different tissue velocity profiles in (b) belong to three individual pixels on the arterial wall of a healthy volunteer as depicted in the ultrasound frame in (a). The curves are part of the dicrotic notch distension feature and exhibit transient behavior from right to left (1 to 3) with respect to peak velocity. Inset: Velocity waveform of the complete cycle, where the *green box* indicates the time spanning the three curves below.

threshold was set to –30 dB. The velocity cutoff for extreme non-physiologic values was set to ±12 mm/s. The size of the 3-D Gaussian kernel was 5 samples × 3 scan lines × 7 frames. Within each ROI, a total of 180 samples along each line were considered for distensibility processing.

RESULTS

The phase-difference method allows extraction of single-pixel tissue motion. Figure 3 is a 3-D representation of CA wall velocity data acquired in this study. Three arbitrary US frames with overlaid velocity data illustrate the in-plane motion. The first frame illustrates the CA during positive distension, the second frame illustrates the CA during negative distension (reduced lumen diameter) and the third frame illustrates again a small distension of the CA. Two cross sections through the walls over time are displayed to highlight the amount and detail of the velocity information present. The total length of this data portion is just half a heart cycle.

Figure 4 illustrates how each pixel contains unique velocity information. In the US image in Figure 4(a), a plane wave B-mode frame is overlaid with tissue velocity data at one particular moment in time. Figure 4(b) illustrates the tissue velocity curves over time at three different positions, indicated by the yellow numbers (1, 2 and 3) in (a) and spaced approximately 15 mm apart. The three velocity curves in Figure 4(b) span a period of 60 ms, with each dot representing a single frame. The peak velocities occur at different time points, a fact attributed to the position of these curves along the wall during a passing arterial pulse wave. The arterial pulse travels from right to left. The *dashed vertical line* in Figure 4(b) indicates the time point of the ultrasound frame. The velocity distension profile in the inset to Figure 4(b) illustrates the complete cycle, and the *box* indicates the origin of the velocity curves below.

Complementary to the previous figure, we illustrate in Figure 5 pixel unique velocity information for a diseased artery wall during the same DN feature. Figure 5(b) illustrates tissue velocity curves at three

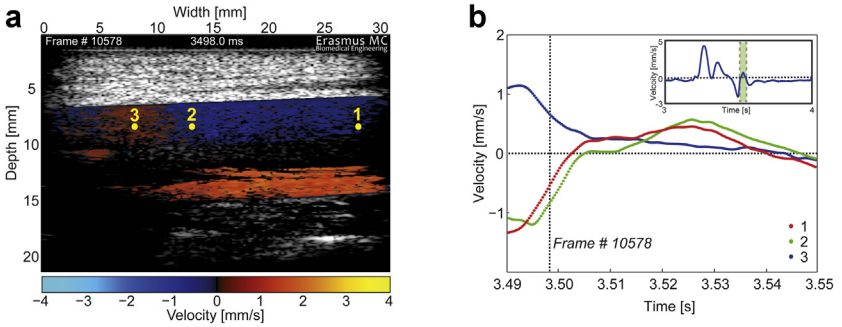

Fig. 5. Pixel unique tissue velocity profiles in a diseased artery wall. Velocity curves 1, 2 and 3 in (b) originate from pixels of the anterior wall of the diseased artery in (a). Pixel 3 belongs to a plaque and exhibits a different course compared with velocity curves 1 and 2.

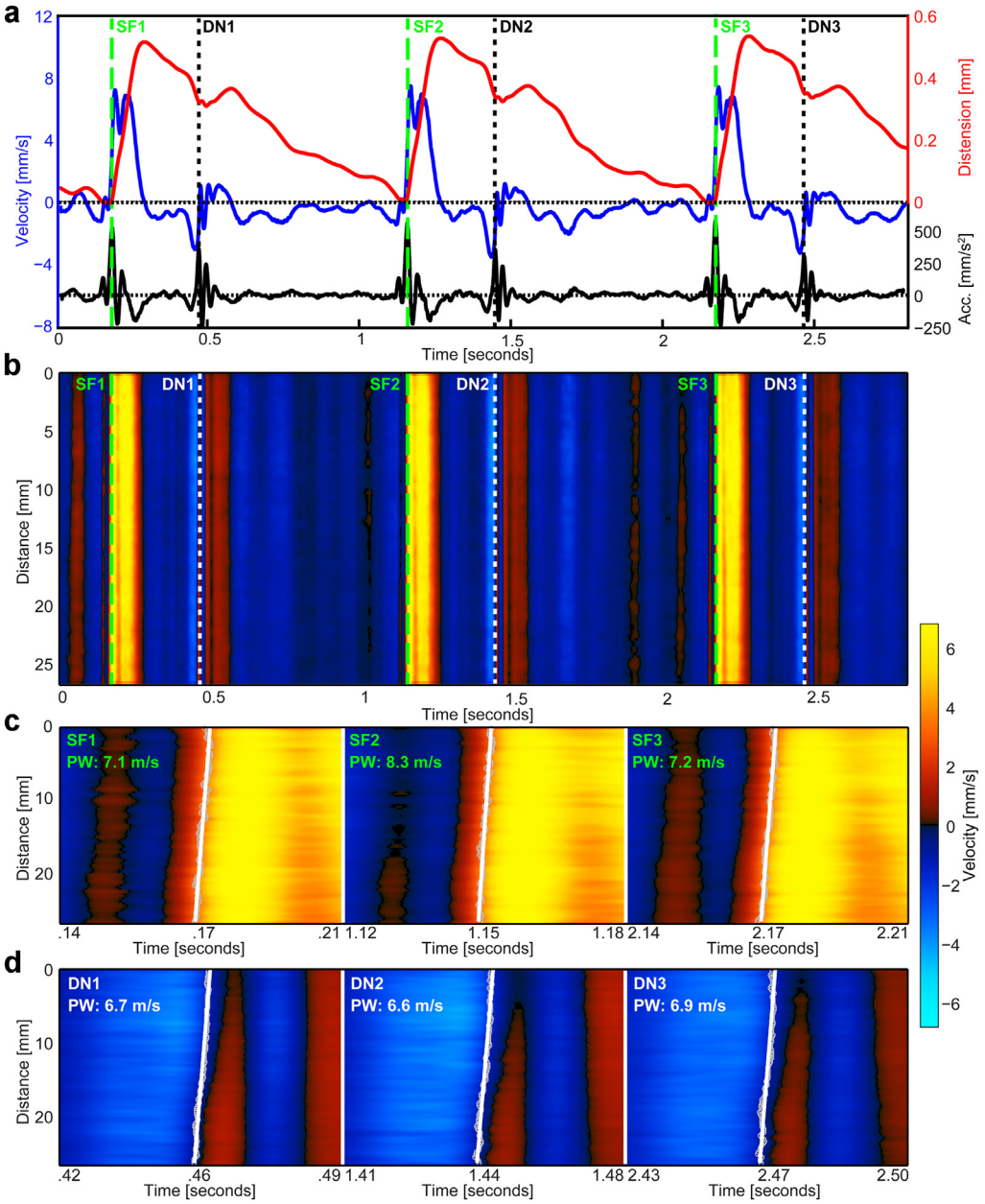

Fig. 6. Measuring pulse wave velocity. (a) Distension, velocity and acceleration curves of a healthy carotid arterial wall. (b) Subtracting the anterior wall velocities from the velocities of the posterior wall yields the distension velocity along the artery wall. The pulse wave velocity can be measured by estimating the slope of transient pulse wave phenomena with respect to time and arterial wall distance. (c, d) Transient pulse wave at the systolic foot and dicrotic notch for three subsequent cardiac cycles, which are magnified subsets of (b).

different positions, where 1 and 2 are located along the thickened intima–media complex and 3 is located on a plaque.

In Figure 6 is the arterial distension velocity waveform obtained by subtracting the velocity of the anterior wall from that of the posterior wall for a typical healthy CA. Figure 6(a) illustrates the distension (*red*), velocity (*blue*) and acceleration (*black*) of the CA. Figure 6(b) illustrates the distension velocity along the artery over time. In Figure 6(c, d) are magnified versions of the distension velocity (Fig. 6b) at the onset (SF, upper three panels) of the waveform and at the dicrotic notch (DN, lower three panels). In the magnified images (Fig. 6a,d) the *gray dots* indicate the peak corresponding to the feature being tracked; the *white lines* are regression lines yielding the PWV in meters per second.

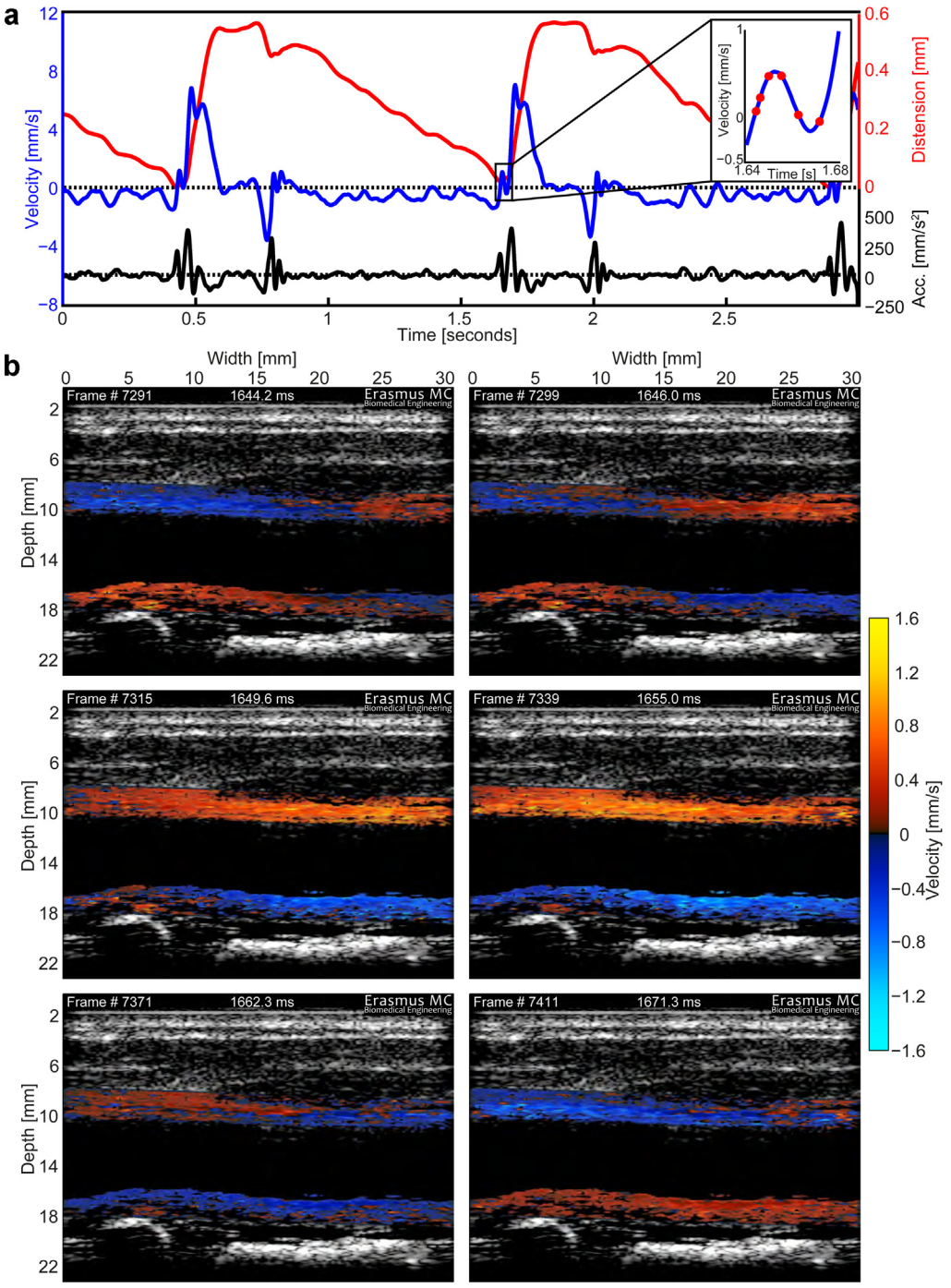

Fig. 7. Imaging transient phenomena along the arterial wall. The interaction of the pulse wave with the carotid artery wall can be visualized with high-frame-rate ultrasound imaging. This figure comprises six individual tissue velocity frames from a healthy carotid artery during a 27-ms episode. The pulse wave comes in from right to left. In (a) are distension waveforms of the same artery. Inset: Small magnified section of the distension waveform, where *red dots* indicate the frames below.

High-frame-rate US imaging combined with the phase-difference method as proposed here allows imaging of tissue motion in great detail. In Figure 7(b) are six different tissue velocity frames from a 4.5-kHz HFR scan of a healthy volunteer. The graphs in Figure 7(a) illustrate the combined distension (*red*), velocity (*blue*) and acceleration (*black*) waveforms of the artery. The *red dots* on the magnified graph (inset) indicate the frames appearing below (Fig.7b). The arbitrarily selected frames 7291, 7299, 7315, 7339, 7371 and 7441 are taken

Table 1. Values of parameters in the high-frame-rate carotid study involving 23 healthy volunteers

Study parameter	Value	Literature value
Carotid artery diameter (mm)	6.1 ± 0.7	5–7[a,h,j]
Distension (%)	5.9 ± 2.1	6–12[h,j]
Velocity (mm/s)		
Minimum	–2.8 ± 0.7	–4[d]
Maximum	5.6 ± 1.6	9–11[d,h]
Acceleration (mm/s^2)		
Minimum	–132 ± 54	–200[d]
Maximum	261 ± 95	500[d]
Pulse wave velocity (m/s)		
Systolic foot	6.8 ± 2.4	3–9[b,c,d,e,f,g,h]
Dicrotic notch	7.7 ± 3.4	3–9[b,e,f,i]
Heart rate (bpm)	62.7 ± 8.4	
Blood pressure (mm Hg)		
Low	74.5 ± 7.5	
High	124.7 ± 8.9	
Age (years)	33.9 ± 9.1	
Body mass index	24.4 ± 3.8	
Female	26%	

[a] Couade et al. 2010.
[b] Couade et al. 2011.
[c] Eriksson et al. 2002.
[d] Hasegawa et al. 2013.
[e] Hermeling et al. 2009.
[f] Kanai et al. 2000.
[g] Luo et al. 2012.
[h] Reesink et al. 2007.
[i] Sorensen et al. 2008.
[j] Tortoli et al. 2006.

around the SF observed in the distension waveform. Other observations from the HFR carotid study involving 23 healthy volunteers can be found in Table 1.

Figure 8 illustrates the results of a HFR US scan, combined with the phase-difference tissue motion method, for a patient with >70% diameter stenosis. In Figure 8(b) are five frames (1540, 3720, 4480, 9832 and 10115) with the instantaneous velocity overlaid on the classic B-mode image. The stenosis can be observed upstream in the images (left side). The bottom right image is an US image of the artery with stenosis obtained using a commercial machine. The superimposed contours indicate the lumen, the plaque location and the field of view that correspond to the HFR frames. The locations of the frames with respect to the overall arterial wall velocity distension are indicated by the *black dashed vertical lines* in Figure 8(a). Frame 1540 exhibits an overall arterial motion (*blue*) that differs from the motion of the plaque (*red*). Frames 3720 and 9832 illustrate the artery at peak positive velocity. Although taken during two different heart cycles, the similarity between the two frames is very apparent. Frame 4480 illustrates the artery at peak negative velocity. Frame 10115 illustrates the artery during the second episode of positive distension velocity, an observation made in this patient only. The combined distension (*red*), velocity (*blue*) and acceleration (*black*) waveforms of the artery as a whole are provided in Figure 8(a).

DISCUSSION

We have described an efficient, high-definition motion-analysis method for assessing tissue dynamics that we applied to measure motion in the wall of the CA. The phase-difference method produces a tissue velocity profile that is unique for each pixel. Integration and differentiation of the tissue velocity profiles with respect to time generate displacement and acceleration profiles. Although the analysis can be applied only if frame-to-frame motion is small ($<<\pi$), for assessment of wall motion in the CA, this condition can easily be met by applying high-frame-rate (HFR) plane-wave imaging.

When combined with the phase-difference method, HFR imaging provides a wealth of information on CA wall motion. Examples of the detailed tissue dynamics that this method can generate are provided in the 3-D representation in Figure 3, in the pulse wave velocity (PWV) close-ups in Figure 6, the velocity snapshots overlaid on the B-mode images in Figures 7 and 8, and, in particular, the raw individual pixel velocities in Figures 4 and 5. We found the detailed motion profiles extracted from the phase difference method to be highly reproducible (see also Figs. 6–8) and in good agreement with those found in the literature (Hermeling et al. 2009; Holdsworth et al. 1999; Kanai et al. 2000; Luo et al. 2012; Sorensen et al. 2008; Tortoli et al. 2006). De Korte et al. (1997) reported before that time delay estimation using the phase-difference method produces results similar to those of the widely used cross-correlation method.

To quantify our image analysis method and to compare it with established methods from the literature, we chose to study the PW in particular. This is a well-studied phenomenon that is readily identifiable in our data. An elaborate example of PW propagation is illustrated in Figure 6(c, d). The PWV was calculated according to the times at which the acceleration peaks arrived along the CA wall. Note that the six PWV values measured during this scan are all different. The average PWV at the SF is 7.5 m/s, and the PWV at the DN is lower, namely, 6.7 m/s. The velocities measured in this individual are somewhat unexpected because they run counter to the expectation that the PWV is higher at the DN than at the SF because of the increased stiffness of the arterial wall at higher systolic pressures (Couade et al. 2010). The averaged data (Table 1) do confirm the expected relation between pressure and PWV. This variance in PWV suggests that a single PWV value is not sufficient to assess the elastic state of the artery (Segers et al. 2009). As argued in the Introduction, an accurate description of the non-linear elasticity of the CA that includes both the PW and other wave-wall interactions (Hasegawa et al. 2013) requires temporal and spatial resolution.

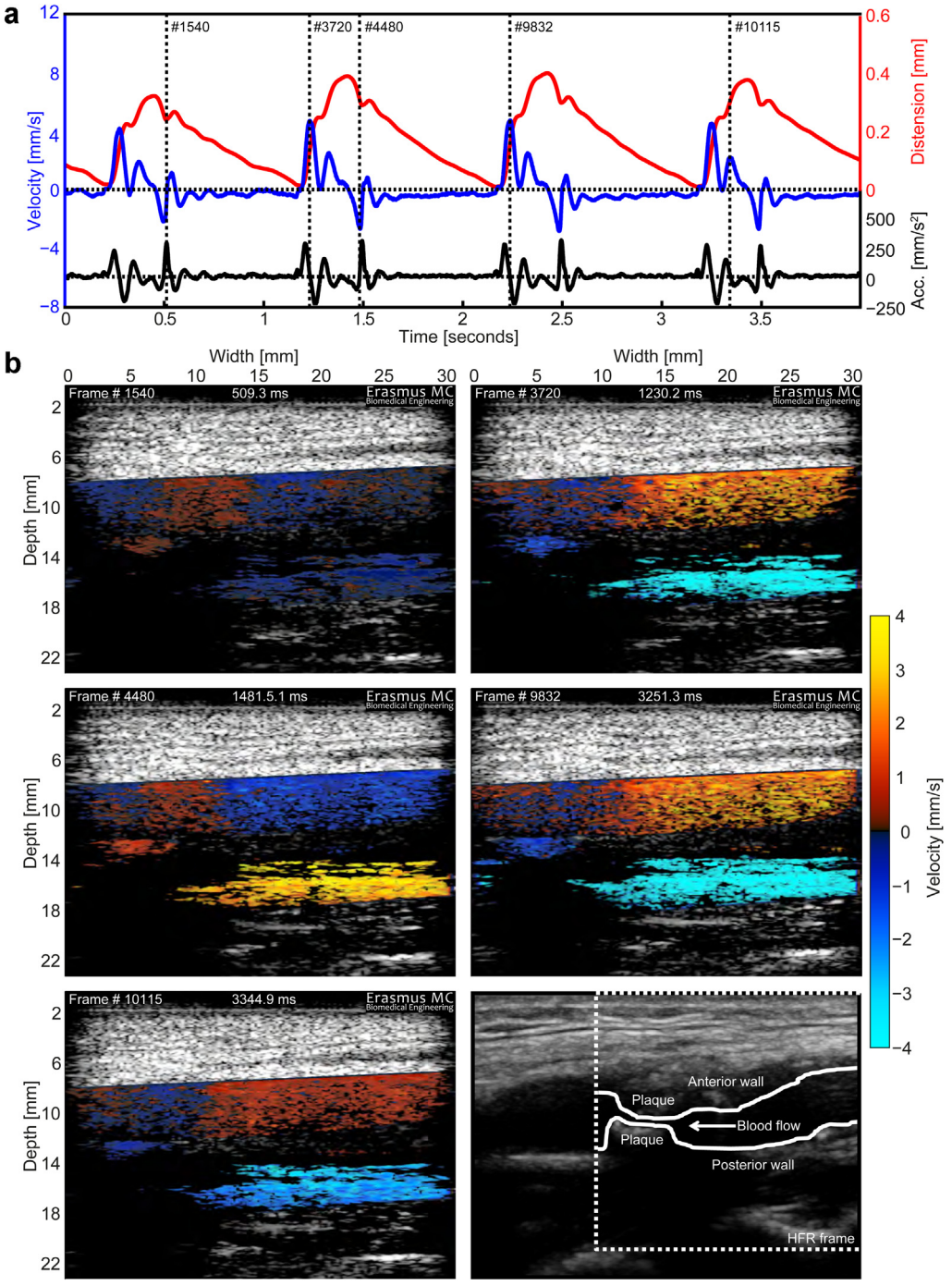

Fig. 8. High-frame-rate imaging of a diseased carotid artery. (a) Distension waveforms of the artery of a patient with a severe carotid artery stenosis (>70%). (b) Five arbitrarily selected tissue velocity frames. The plaque observed at the left side of these frames exhibits distinct tissue velocity with respect to the anterior and posterior wall. The bottom right ultrasound frame in (b) was obtained with a commercial ultrasound scanner. Overlaid contours indicate the lumen, the plaque location and the field of view that corresponds to the high-frame-rate frames.

Our method provides both spatial and temporal resolution, as indicated in the visualization of the transient interaction of the incident PW with the arterial wall. In Figure 7(b) are six discrete velocity frames around the onset of the distension waveform. As the PW enters from right to left, the artery expands slightly and contracts again within a 20-ms period. At an acquisition frame rate of 4.5 kHz, this event spans approximately 90 frames, whereas the interaction of the wall with the incoming phase of the PW covers about 20 frames.

During this interaction, we measured tissue displacements on the order of 1 μm. Sorensen et al. (2008) have previously suggested that going beyond the 1-kHz frame rate is not necessary to estimate PWV. Although such a low frame rate might allow for a simple estimate of the cycle-averaged PWV in an entire segment, it is certainly not enough for a full assessment of artery wall dynamics, as we have indicated in this study.

The high-speed tissue motion observed in healthy patients provides a baseline for comparison with diseased arteries. Figures 5 and 8 illustrate the first result of this exploration. Although the three velocity curves in Figure 5 and the five frames (out of >12,000) in Figure 8 can by no means cover all the features that were observed during this 4-s scan, they do illustrate that the movement of a diseased artery is completely different from that of a healthy artery (compare Figs. 4 and 5). The five frames in Figure 8 illustrate how a heavily calcified plaque (calcification was confirmed by computed tomography scan) moves together with the posterior wall and generates sharp velocity gradients with the anterior wall. It is likely that a strain analysis would reveal a region of high strain around the plaque where it moves relative to the anterior wall. As well as this difference in artery movement, there is also a marked difference in the distension profiles between the healthy volunteers (Figs. 6 and 7) and the atherosclerotic patient (Fig. 8). Although the distension velocity profile of the two volunteers (*blue curve*) first comprises a large positive velocity pulse followed by a negative one, the profile of the patient contains a characteristic pair of positive pulses, with a moment of zero velocity inbetween. This reproduces the "late systolic peak" commonly observed in aging and associated with increased wave reflection (Kelly et al. 1989). The velocity distension cycle concludes with a slow recovery during diastole. A patient study in a larger cohort is needed to further qualify and quantify to what extent the dynamics in diseased arteries differ from the dynamics observed in healthy arteries.

Analysis of the scans from the healthy volunteers (n = 46, 23 volunteers, each with two CAs) revealed that there are several factors during acquisition and data processing that affect the quality of our results. First, for accurate PWV determination, the artery must be precisely aligned with the transducer surface, and the image should show the lumen at maximum diameter. This view corresponds to a cross-sectional view straight through the middle of the CA. A good predictor of a successful scan is observation of the intima–media complex. Second, finding a good view was complicated by the low frame rate of the preview mode. Because not all scans in this study met these criteria, in some cases (4 of 46) it was not possible to obtain a reliable PWV. Third, we found PWV estimation to be strongly influenced by the characteristics of the low-pass filter applied to the scan lines, a finding similar to that of Hermeling et al. (2007, 2008). Finally, in many cases we observed that the posterior wall motion is stronger than that of the anterior wall, which is most likely caused by transducer pressure on the tissue overlying the CA.

By combining HFR US imaging with the proposed phase-difference method, we were able to monitor all CA wall dynamics throughout the cardiac cycle. This method allowed us to observe various dynamic phenomena, including PW propagation, PW–wall interaction, layer compression and wave reflections. We also illustrated that the tissue velocity fields in healthy and diseased arteries are different. These velocity fields can be used to calculate local strain and strain rate, factors that are directly related to local elasticity and that have proven utility in several clinical applications. Despite their utility, in this study we did not consider local strain and strain rate, because a better understanding of the lateral tissue motion component is required before the strain can be accurately computed.

CONCLUSIONS

The natural local deformations of the human carotid artery wall include displacements in sub-micrometer dimensions on a sub-millisecond time scale. In this study, we have described that these slight and rapid deformations can be captured by means of high-frame-rate ultrasound imaging together with a newly developed phase-difference method. This method is extremely efficient in computational terms and offers high temporal and spatial resolution. By screening the carotid arteries of a group of healthy volunteers and two patients with atherosclerosis, we have found that high-frame-rate imaging can visualize tissue dynamics in unprecedented detail.

Acknowledgments—The authors thank Robert Beurskens, Geert Springeling and Michiel Manten for their technical support.

REFERENCES

Asmar R, Benetos A, Topouchian J, Laurent P, Pannier B, Brisac AM, Target R, Levy BI. Assessment of arterial distensibility by automatic pulse wave velocity measurement validation and clinical application studies. Hypertension 1995;263:485–490.

Benthin M, Dahl P, Ruzicka R, Lindström K. Calculation of pulse-wave velocity using cross correlation: Effects of reflexes in the arterial tree. Ultrasound Med Biol 1991;17:461–469.

Carr S, Farb A, Pearce WH, Virmani R, Yao JS. Atherosclerotic plaque rupture in symptomatic carotid artery stenosis. J Vasc Surg 1996; 235:755–766.

Cheng GC, Loree HM, Kamm RD, Fishbein MC, Lee RT. Distribution of circumferential stress in ruptured and stable atherosclerotic lesions: A structural analysis with histopathological correlation. Circulation 1993;874:1179–1187.

Cheng J, Lu J. Extended high-frame rate imaging method with limited-diffraction beams. IEEE Trans Ultrason Ferroelectr Freq Control 2006;53:880–899.

Couade M, Pernot M, Messas E, Emmerich J, Hagège A, Fink M, Tanter M. Ultrafast imaging of the arterial pulse wave. IRBM 2011;32:106–108.

Couade M, Pernot M, Prada C, Messas E, Emmerich J, Bruneval P, Criton A, Fink M, Tanter M. Quantitative assessment of arterial wall biomechanical properties using shear wave imaging. Ultrasound Med Biol 2010;36:1662–1676.

De Korte C, Sierevogel M, Mastik F, Strijder C, Schaar J, Velema E, Pasterkamp G, Serruys P, van der Steen A. Identification of atherosclerotic plaque components with intravascular ultrasound elastography in vivo a Yucatan pig study. Circulation 2002;105:1627–1630.

De Korte C, Van der Steen A, Dijkman B, Lancée C. Performance of time delay estimation methods for small time shifts in ultrasonic signals. Ultrasonics 1997;35:263–274.

D'Hooge J, Heimdal A, Jamal F, Kukulski T, Bijnens B, Rademakers F, Hatle L, Suetens P, Sutherland G. Regional strain and strain rate measurements by cardiac ultrasound: Principles, implementation and limitations. Eur J Echocardiogr 2000;13:154–170.

Ekroll I, Swillens A, Segers P, Dahl T, Torp H, Lovstakken L. Simultaneous quantification of flow and tissue velocities based on multi-angle plane wave imaging. IEEE Trans Ultrason Ferroelectr Freq Control 2013;60:727–738.

Eriksson A, Greiff E, Loupas T, Persson M, Pesque P. Arterial pulse wave velocity with tissue Doppler imaging. Ultrasound Med Biol 2002;285:571–580.

Fung Y. Biomechanics: Mechanical properties of living tissues. New York: Springer; 1993.

Golemati S, Sassano A, Lever MJ, Bharath AA, Dhanjil S, Nicolaides AN. Carotid artery wall motion estimated from B-mode ultrasound using region tracking and block matching. Ultrasound Med Biol 2003;29:387–399.

Grønholdt MLM. Ultrasound and lipoproteins as predictors of lipid-rich, rupture-prone plaques in the carotid artery. Arterioscler Thromb Vasc Biol 1999;19:2–13.

Grønholdt MLM, Nordestgaard BG, Schroeder TV, Vorstrup S, Sillesen H. Ultrasonic echolucent carotid plaques predict future strokes. Circulation 2001;104:68–73.

Hartley CJ, Litowitz H, Rabinovitz RS, Zhu WX, Chelly JE, Michael LH, Bolli R. An ultrasonic method for measuring tissue displacement: Technical details and validation for measuring myocardial thickening. IEEE Trans Biomed Eng 1991;38:735–747.

Hasegawa H, Hongo K, Kanai H. Measurement of regional pulse wave velocity using very high frame rate ultrasound. J Med Ultrason 2013;40:91–98.

Hasegawa H, Kanai H. Simultaneous imaging of artery-wall strain and blood flow by high frame rate acquisition of RF signals. IEEE Trans Ultrason Ferroelectr Freq Control 2008;55:2626–2639.

Heimdal A, Støylen A, Torp H, Skjærpe T. Real-time strain rate imaging of the left ventricle by ultrasound. J Am Soc Echocardiogr 1998;11:1013–1019.

Hellings WE, Peeters W, Moll FL, Piers SR, van Setten J, Van der Spek PJ, de Vries JPP, Seldenrijk KA, De Bruin PC, Vink A, Velema E, de Kleijn DP, Pasterkamp G. Composition of carotid atherosclerotic plaque is associated with cardiovascular outcome a prognostic study. Circulation 2010;121:1941–1950.

Hermeling E, Reesink K, Kornmann L, Reneman R, Hoeks A. The dicrotic notch as alternative time-reference point to measure local pulse wave velocity in the carotid artery by means of ultrasonography. J Hypertension 2009;27:2028.

Hermeling E, Reesink KD, Reneman RS, Hoeks AP. Measurement of local pulse wave velocity: Effects of signal processing on precision. Ultrasound Med Biol 2007;33:774–781.

Hermeling E, Reesink KD, Reneman RS, Hoeks AP. Confluence of incident and reflected waves interferes with systolic foot detection of the carotid artery distension waveform. J Hypertension 2008;26:2374–2380.

Hermeling E, Reneman RS, Hoeks AP, Reesink KD. Advances in arterial stiffness assessment. Artery Res 2011;54:130–136.

Hoeks A, Brands P, Smeets F, Reneman R. Assessment of the distensibility of superficial arteries. Ultrasound Med Biol 1990;16:121–128.

Holdsworth D, Norley C, Frayne R, Steinman D, Rutt B. Characterization of common carotid artery blood-flow waveforms in normal human patients. Physiol Meas 1999;20:219–240.

Inaba Y, Chen J, Bergmann S. Carotid plaque, compared with carotid intima-media thickness, more accurately predicts coronary artery disease events: A meta-analysis. Atherosclerosis 2012;220:128–133.

Jensen JA, Munk P. A new method for estimation of velocity vectors. IEEE Trans Ultrason Ferroelectr Freq Control 1998;45:837–851.

Kanai H, Umezawa A, Koiwa Y. Transcutaneous measurement of frequency dispersion in the regional pulse wave velocity. In: Proceedings, 2000 IEEE International Ultrasonics Symposium, Puerto Rico, 22–25 October. New York: IEEE, 2000;2:1281–1284.

Kelly R, Hayward C, Avolio A, O'Rourke M. Noninvasive determination of age-related changes in the human arterial pulse. Circulation 1989;80:1652–1659.

Koivistoinen T, Kööbi T, Jula A, Hutri-Kähönen N, Raitakari O, Majahalme S, Kukkonen-Harjula K, Lehtimäki T, Reunanen A, Viikari J, Turjanmaa V, Nieminen T, Kähönen M. Pulse wave velocity reference values in healthy adults aged 26–75 y. Clin Physiol Funct Imaging 2007;27:191–196.

Korteweg D. Ueber die fortpflanzungsgeschwindigkeit des schalles in elastischen röhren. Ann Phys 1878;241:525–542.

Kruizinga P, Mastik F, de Jong N, van der Steen A, van Soest G. Plane-wave ultrasound beamforming using a nonuniform fast Fourier transform. IEEE Trans Ultrason Ferroelectr Freq Control 2012a;59:2684–2691.

Kruizinga P, Mastik F, de Jong N, van der Steen AF, van Soest G. High frame rate ultrasound imaging of human carotid artery dynamics. In: Proceedings, 2012 IEEE International Ultrasonics Symposium, Dresden, Germany, 7–10 October, New York: IEEE, 2012b:1177–1180.

Lantelme P, Mestre C, Lievre M, Gressard A, Milon H. Heart rate: An important confounder of pulse wave velocity assessment. Hypertension 2002;39:1083–1087.

Laurent S, Cockcroft J, Van Bortel L, Boutouyrie P, Giannattasio C, Hayoz D, Pannier B, Vlachopoulos C, Wilkinson I, Struijker-Boudier H. Expert consensus document on arterial stiffness: Methodological issues and clinical applications. Eur Heart J 2006;27:2588–2605.

Lorenz M, Markus H, Bots M, Rosvall M, Sitzer M. Prediction of clinical cardiovascular events with carotid intima-media thickness a systematic review and meta-analysis. Circulation 2007;115:459–467.

Lu J. 2D and 3D high frame rate imaging with limited diffraction beams. IEEE Trans Ultrason Ferroelectr Freq Control 1997;44:839–856.

Lubinski MA, Emelianov SY, O'Donnell M. Speckle tracking methods for ultrasonic elasticity imaging using short-time correlation. IEEE Trans Ultrason Ferroelectr Freq Control IEEE 1999;46:82–96.

Luo J, Li R, Konofagou E. Pulse wave imaging of the human carotid artery: An in vivo feasibility study. IEEE Trans Ultrason Ferroelectr Freq Control 2012;59:174–181.

O'Rourke M, Staessen J, Vlachopoulos C, Duprez D, Plante GE. Clinical applications of arterial stiffness: Definitions and reference values. Am J Hypertension 2002;15:426–444.

Reesink KD, Hermeling E, Hoeberigs MC, Reneman RS, Hoeks AP. Carotid artery pulse wave time characteristics to quantify ventriculoarterial responses to orthostatic challenge. J Appl Physiol 2007;102:2128–2134.

Schaar J, de Korte C, Mastik F, Strijder C, Pasterkamp G, Boersma E, Serruys P, van der Steen A. Characterizing vulnerable plaque features with intravascular elastography. Circulation 2003;108:2636–2641.

Schmidt-Trucksäss A, Grathwohl D, Schmid A, Boragk R, Upmeier C, Keul J, Huonker M. Assessment of carotid wall motion and stiffness with tissue Doppler imaging. Ultrasound Med Biol 1998;24:639–646.

Segers P, Kips J, Trachet B, Swillens A, Vermeersch S, Mahieu D, Rietzschel E, De Buyzere M, Van Bortel L. Limitations and pitfalls

of non-invasive measurement of arterial pressure wave reflections and pulse wave velocity. Artery Res 2009;32:79–88.
Shadwick RE. Mechanical design in arteries. J Exp Biol 1999;202: 3305–3313.
Shah PK. Mechanisms of plaque vulnerability and rupture. J Am Coll Cardiol 2003;41(4, Suppl. 1):S15–S22.
Shahmirzadi D, Konofagou E. Detection of aortic wall inclusions using regional pulse wave propagation and velocity in silico. Artery Res 2012;6.
Shoji T, Maekawa K, Emoto M, Okuno S, Yamakawa T, Ishimura E, Inaba M, Nishizawa Y. Arterial stiffness predicts cardiovascular death independent of arterial thickness in a cohort of hemodialysis patients. Atherosclerosis 2010;210:145–149.
Sorensen G, Jensen J, Udesen J, Holfort I, Jensen J. Pulse wave velocity in the carotid artery. In: Proceedings, 2008 IEEE International Ultrasonics Symposium, Beijing, China, 2–4 November. New York: IEEE, 2008:1386–1389.
Tanter M, Bercoff J, Sandrin L, Fink M. Ultrafast compound imaging for 2-D motion vector estimation: Application to transient elastography. IEEE Trans Ultrason Ferroelectr Freq Control 2002;49: 1363–1374.
Tortoli P, Morganti T, Bambi G, Palombo C, Ramnarine KV. Noninvasive simultaneous assessment of wall shear rate and wall distension in carotid arteries. Ultrasound Med Biol 2006;32:1661–1670.
Triposkiadis F, Sitafidis G, Kostoulas J, Skoularigis J, Zintzaras E, Fezoulidis I. Carotid plaque composition in stable and unstable coronary artery disease. Am Heart J 2005;150:782–789.
Udesen J, Gran F, Hansen K, Jensen JA, Thomsen C, Nielsen MB. High frame-rate blood vector velocity imaging using plane waves: Simulations and preliminary experiments. IEEE Trans Ultrason Ferroelectr Freq Control 2008;55:1729–1743.
Van Popele N, Grobbee D, Bots M, Asmar R, Topouchian J, Reneman R, Hoeks A, van der Kuip D, Hofman A, Witteman J. Association between arterial stiffness and atherosclerosis: The Rotterdam Study. Stroke 2001;32:454–460.
Wilson LS, Robinson DE. Ultrasonic measurement of small displacements and deformations of tissue. Ultrason Imaging 1982;4: 71–82.
Zahnd G, Orkisz M, Sérusclat A, Moulin P, Vray D. Evaluation of a Kalman-based block matching method to assess the bi-dimensional motion of the carotid artery wall in B-mode ultrasound sequences. Med Image Anal 2013;17:573–585.